

We are IntechOpen, the world's leading publisher of Open Access books Built by scientists, for scientists

6,900

Open access books available

186,000

International authors and editors

200M

Downloads

Our authors are among the

154

Countries delivered to

TOP 1%

most cited scientists

12.2%

Contributors from top 500 universities



WEB OF SCIENCE™

Selection of our books indexed in the Book Citation Index
in Web of Science™ Core Collection (BKCI)

Interested in publishing with us?
Contact book.department@intechopen.com

Numbers displayed above are based on latest data collected.
For more information visit www.intechopen.com



Fluid Instabilities and Transition to Turbulence

Michael S. Roberts

Abstract

Fluid instabilities show up in many places in everyday life, nature and engineering applications. An often seemingly stable system with a gradient will often give rise to the development of instability, which can cascade eventually into turbulence. Governed by the parameters of the flow and fluids, when exposed to perturbation in the system, some wavelengths will grow, while others will not. This selectivity of specific structure sizes can be determined by using linear stability theory and then accounting for viscosity. Once these unstable wavelengths have grown to a substantial degree, the system typically becomes nonlinear before turbulence eventually sets in. Initially, looking at buoyancy-driven instabilities, one can clearly see how certain wavelengths can be selected. This can be extended to shear-driven instabilities and to geophysical systems. For some flows, simplifications can be made to analyze the specific fluid structures, while for others, only broad conclusions can be drawn about the stability criteria. With parallel shear flows (like that over wings and through pipes), the applications are more obvious, but the equations more difficult. However, conclusions can be drawn as to how one can control, prevent and initiate instability to suit our engineering needs.

Keywords: instability, turbulence, transition, Rayleigh-Taylor, Richtmyer-Meshkov, Kelvin-Helmholtz, Orr-Sommerfeld

1. Introduction

Fluid instabilities show up everywhere in nature. Fluid flow will start off laminar and smooth and then quickly transition to an irregular pattern eventually transitioning to turbulence. All you have to do to see its prevalence is look up at the sky on a cloudy day when the conditions are right such that there will be large clouds rolling past one another and spirals develop. This is the Kelvin-Helmholtz instability (where there is a shear between two fluids with different relative velocities). Another common instability is when you add cold milk to hot tea. The larger density of the cold fluid falls and displaces the hotter less dense fluid, and it is clear that specific structures form. A similar phenomenon occurs for contained flows, such as in pipes, or as in unbounded flow, such as that over a wing or out of a faucet. In all of these cases, solving too simplified equations of motion would lead to the solution that our ignorant view of the world might expect, where the fluids retain their smooth laminar structure, but this does not happen. Instead a specific size and shape of structure forms, usually in a periodic fashion, and this structure grows

until finally becoming more and more chaotic until the flow is not longer laminar, but has transitioned to turbulence. A normal mode analysis can often be performed (where the equations of motion are assumed to be in a form where different wavelengths can be tested), and through solving the equation, the growth rate of various wavelength is found. This will tell us what specific configuration is expected.

When engineering new devices that involve fluid flows, it is important to account for these instabilities. This can be to try and minimize the onset of turbulence (or speed it up) or to understand the different wavelengths that may form and possibly causes resonances or unwanted behavior.

2. Stratified fluid instabilities

From a fluid instability perspective, stratified fluid systems are in some ways the easiest to understand and visualize, so we will start there. It is often the case when there is a fluid system in which two fluids with different properties, an unstable configuration can be realized. Here we will mainly consider the case where there is a clear boundary between two fluids, but this concept can be extended to a continuous variation between fluids, but the diffusion effects would damp out any perturbation and instability, so would not be as pronounced.

We can start our discussion by taking a vorticity perspective to the instability growth. If we start in two-dimensions with the inviscid Navier-Stokes equation and add a background velocity base state to the perturbed equation (here we are considering small perturbations to the base state), some conclusions can be drawn although not a rigorous derivation.

$$\frac{\partial \vec{u}}{\partial t} + \vec{u} \cdot \nabla \vec{u} = -\frac{1}{\rho} \nabla P \Rightarrow \frac{\partial u_x + U_x}{\partial t} + (u_x + U_x) \frac{\partial (u_x + U_x)}{\partial x} + \frac{\partial u_y}{\partial t} + u_y \frac{\partial u_y}{\partial y} = -\frac{1}{\rho} \nabla P \quad (1)$$

In Eq. 1, where u and U are the velocities of the perturbation and base state, respectively, ρ is the density and P is the pressure. We will neglect products of small quantities and also subtract the equation for the background flow. This will leave us with an extra term representing the product of our base velocity and perturbed velocity. We will now take the curl of this equation to arrive at a representation of the vorticity.

$$\nabla \times \left\{ \frac{\partial u_x + U_x}{\partial t} + (u_x + U_x) \frac{\partial (u_x + U_x)}{\partial x} + \frac{\partial u_y}{\partial t} + u_y \frac{\partial u_y}{\partial y} = -\frac{1}{\rho} \nabla P \right\} \quad (2)$$

$$\Rightarrow \frac{D\vec{\omega}}{Dt} + \nabla \times \left(U_x \frac{\partial u_x}{\partial x} \hat{i} \right) + \nabla \times \left(-\rho^{-1} \nabla P \right) \quad (3)$$

The expansion of the extra vorticity production term from the base velocity gives a few terms that can be neglected for this discussion $\Rightarrow \left(\frac{\partial}{\partial x} - \frac{\partial}{\partial y} \right) U_x \frac{\partial u_x}{\partial x} \hat{i} \Rightarrow -\frac{\partial U_x}{\partial y} \frac{\partial u_x}{\partial x}$. We will consider second-order derivatives of the perturbed quantities small enough to be neglected. We have also neglected the nonlinear convective terms coming out of the vorticity equation for simplicity. This yields:

$$\frac{D\vec{\omega}}{Dt} = \frac{1}{\rho^2} \nabla \rho^2 \times \nabla P + \frac{\partial U_x}{\partial y} \frac{\partial u_x}{\partial x} \quad (4)$$

From this we see that a pressure gradient across a density gradient can create vorticity (this is a buoyancy-driven instability) and a velocity gradient can create vorticity as well (shear-driven instability). Both of these require a perturbation at the interface to develop.

2.1 Buoyancy-driven instabilities

Buoyancy-driven fluid instabilities occur in a stratified fluid system when the light fluid is accelerated into the heavier one often by means of a pressure gradient. One way to understand this form of instability is from the baroclinic torque present at the stratified, perturbed interface. This baroclinic torque is created from the misalignment of the pressure and density gradients at the perturbed interface. When in the unstable configuration, for a particular harmonic component of the initial perturbation, this torque between the two fluids will create vorticity. This vorticity will impose a velocity field that will tend to increase the misalignment of the gradient vectors, which in turn will create additional vorticity, leading to more misalignment. This is observed in Eq. 4, where if we neglect the velocity gradient in the base flow as we have not considered that here, an increase in vorticity will be realized if $\frac{1}{\rho^2} \nabla \rho \times \nabla P$, which means that for instability $\nabla P \cdot \nabla \rho < 0$.

Illustrated in **Figure 1**, it is observed that the two counter-rotating vortices with strength ω have velocity fields that sum at the peak and trough of the perturbed interface. In the stable configuration the vorticity, and thus the induced velocity field, will be in a direction that decreases the misalignment and therefore stabilizes the system. In order for the instability to develop, $\nabla P \cdot \nabla \rho < 0$. This pressure is increasing in the direction from the more dense to the less dense fluid.

Two specific buoyancy-driven instabilities are the Rayleigh-Taylor (characterized by a constant acceleration) and Richtmyer-Meshkov (characterized by an impulsive acceleration).

2.1.1 Rayleigh-Taylor instability

The Rayleigh-Taylor instability (RTI) is a buoyancy-driven instability where the acceleration is constant with respect to the fluid flow time. The most notable example of the Rayleigh-Taylor instability is when a heavy fluid lies atop a light one while in the presence of a downward acting gravitational field. This instability is displayed in **Figure 2** of the experimental images of Roberts [1]. Here, the initially light over heavy stable fluid configuration is made unstable by accelerating the

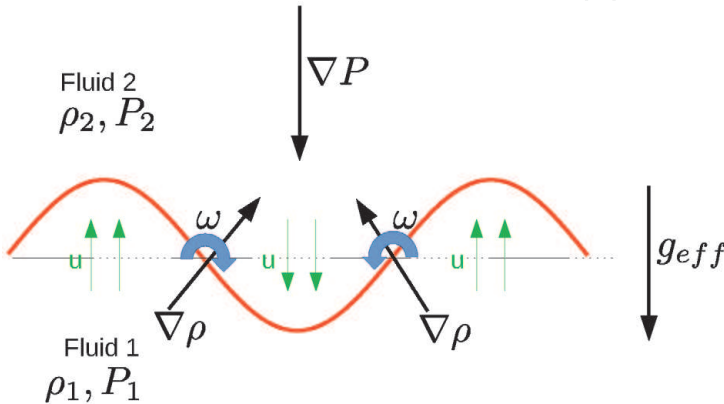


Figure 1.
Visualization of an unstable buoyancy instability configuration where baroclinic torque at the interface creates vorticity and induces a velocity field that increases the baroclinic torque.

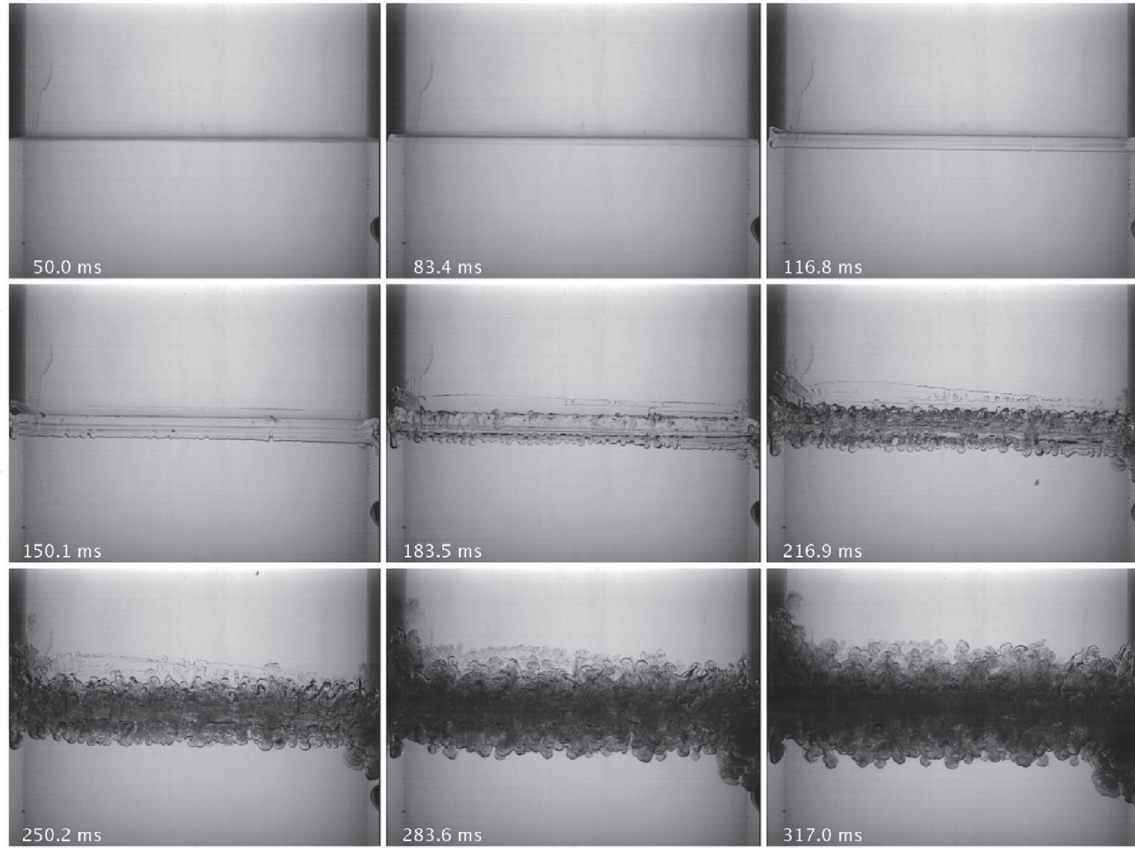


Figure 2. Experimental images of Roberts [1] in which an unstable Rayleigh-Taylor configuration is formed where the light over heavy fluid system is made unstable. A progression of a specific wavelength is observed to develop and eventually a turbulent mixing region.

system downward at a rate greater than gravity (essentially switching the direction of gravity so that it is upward). As can be seen, a specific wavelength appears out of the background which grows and eventually creates a turbulent mixing region.

A simplified way to understand how we may have a Rayleigh-Taylor (RT) stable (or unstable) stratified configuration is by considering the situation in which there is an acceleration g_{eff} acting downward (in the negative z direction) on a stratified fluid system as depicted in **Figure 3** [1]. Considering a fluid particle, we can look at the forces acting on it in reference to the coordinate system in which z is directed upward. The acceleration produces a pressure gradient $\frac{\partial P}{\partial z} = -\rho g_{\text{eff}}$ inside the fluid which may create a force imbalance upon the fluid particle. If we choose a fluid particle in the upper fluid with density ρ_2 , we see that the force, due to pressure, at the lower surface of this particle would be $[P_0 - \rho_1 g_{\text{eff}} \ell - \rho_2 g_{\text{eff}} (z - \ell)]A$ (where A is the area) and would be $[P_0 - \rho_1 g_{\text{eff}} \ell - \rho_2 g_{\text{eff}} (z - \ell + \Delta z)]A$ for the upper surface. We have chosen the geometry of the fluid particle here to simplify the equations. The force due to gravity on the fluid particle is $-\rho_2 \nabla g_{\text{eff}} = -\rho_2 \Delta z A g_{\text{eff}}$ (where ∇ is the volume). Writing out Newton's second law we have (lower pressure force – upper pressure force + gravity force = mass \times acceleration),

$$F = m\ddot{z} = \rho_2 g_{\text{eff}} \Delta z A - \rho_2 g_{\text{eff}} \Delta z A = (\rho_2 \nabla + \rho_1 \beta) \frac{d^2 z}{dt^2} = 0, \quad (5)$$

where we have also included the added mass $\rho_1 \beta$ to account for the other fluid that must be accelerated away with the fluid particle. For this configuration, the fluid particle does not move, which is expected. If we interchange the fluid particle

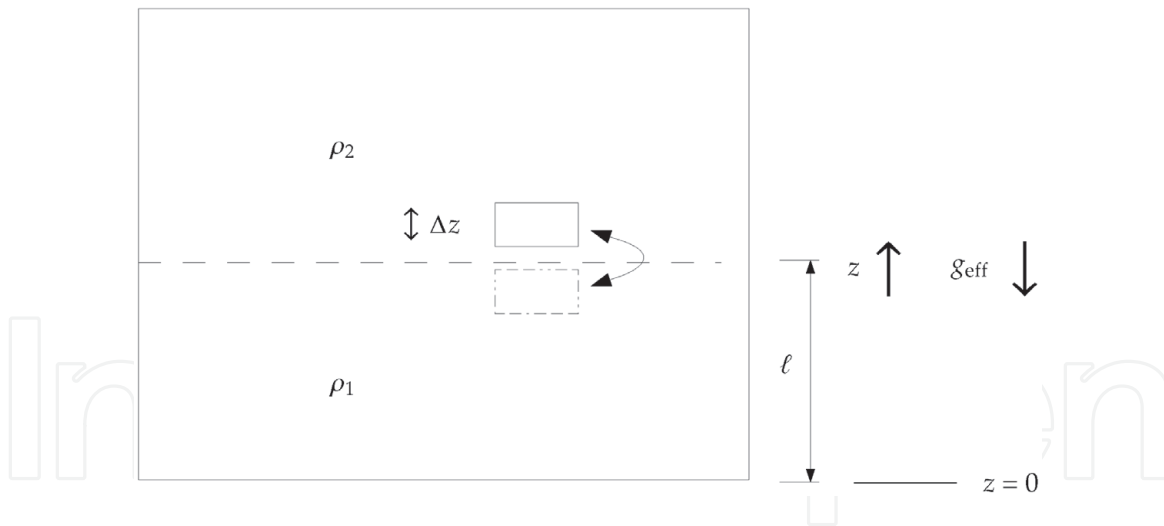


Figure 3.

A fluid particle in the upper fluid is interchanged with one from the lower fluid in a stratified system with downward acting acceleration [1]. Once displaced to the bottom fluid, the force balance on the particle might yield a configuration where it will continue to move from equilibrium. If $\rho_2 > \rho_1$, the fluid particle is accelerated further downward and the system is unstable. If $\rho_2 < \rho_1$, the fluid particle is pushed back across the interface and the system is stable.

with one from the lower fluid where the density is ρ_1 , from Newton's second law, for the initial particle, we obtain (noting that the pressure forces have changed since we are in the lower fluid),

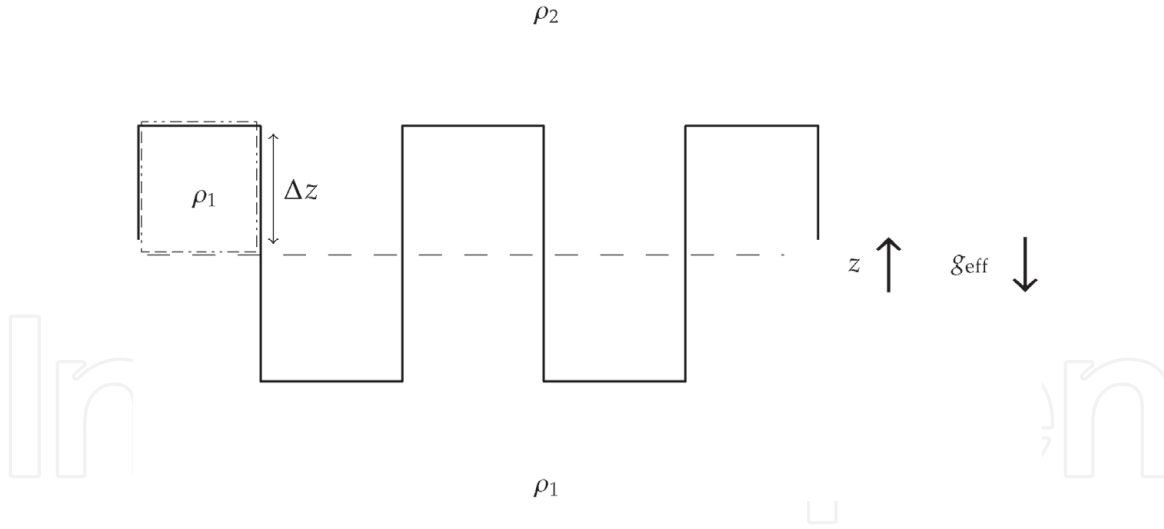
$$\begin{aligned} & \{ [P_0 - \rho_1 g_{\text{eff}} z] A - [P_0 - \rho_1 g_{\text{eff}} (z + \Delta z)] A \} - \rho_2 g_{\text{eff}} \Delta z A \\ & = \rho_1 g_{\text{eff}} \Delta z A - \rho_2 g_{\text{eff}} \Delta z A = (\rho_2 \nabla + \rho_1 \beta) \frac{d^2 z}{dt^2}. \end{aligned} \quad (6)$$

From this, if $\rho_1 > \rho_2$, the fluid particle is pushed back to where it came from (the system is stable). However, if $\rho_2 > \rho_1$, the fluid particle is pushed further away from where it originated and the system is unstable.

This concept of a fluid particle moving across the interface resulting in instability can be extended to the deflection of an interface in the Rayleigh-Taylor instability and illustrates the necessity of an initial perturbation on the interface since there is no mechanism to interchange a fluid particle across the interface. An example of a simple interface is shown in **Figure 4**, where the coordinate system is the same as in **Figure 3**. The interface has been deformed, simulating perturbations on the interface. For simplicity the geometry of the interface deformation has been chosen to be rectangular (the derivation here can be generalized to an individual Fourier mode so that any interface deformation would follow the same behavior). The fluid particle relocation is caused by deformation of the interface. The pressure force on the fluid particle's lower surface is $[P_0 - \rho_1 g_{\text{eff}} \ell] A$ and is $[P_0 - \rho_1 g_{\text{eff}} \ell - \rho_2 g_{\text{eff}} \Delta z] A$ for the upper surface. The force due to the weight of the fluid particle (which has density ρ_1) is $-\rho_1 \nabla g_{\text{eff}} = -\rho_1 \Delta z A g_{\text{eff}}$. Note that once again we have chosen the interface deformation shape to simplify the calculations. We can then form the equation for the force balance as,

$$\rho_2 g_{\text{eff}} \Delta z A - \rho_1 g_{\text{eff}} \Delta z A = (\rho_1 \nabla + \rho_2 \beta) \frac{d^2 z}{dt^2}. \quad (7)$$

In this arrangement, if $\rho_1 > \rho_2$, the fluid particle is pushed back to its original position (and thus the interface is brought back to equilibrium, so the system is

**Figure 4.**

Here an interface is shown [1] downward acting acceleration of a fluid particle displaced from the lower to upper fluid by means of interface deformation. If $\rho_2 > \rho_1$, the system is unstable (the fluid particle moves up farther from the center further deforming the interface). If $\rho_2 < \rho_1$, the fluid particle is moved back toward the center and the system is stabilized.

stable). However, if $\rho_2 > \rho_1$, the fluid particle is pushed further away from where it originated (deforming the interface further) and thus the system is unstable.

From this derivation, it is seen how the instability progresses, but does not say much about the initial stages (for that we need to use linear stability theory, Section 2.1.4) or late time. For the late time development, from Eq. (7), we can make some back of the envelope assumptions and arrive at a well known expression for the late time turbulent Rayleigh-Taylor instability. If we assume β in the added mass is the same as the Volume and rearrange and integrate twice, we can arrive at the well known expression:

$$h = \alpha A g t^2, \quad (8)$$

where α is the growth constant and A is the Atwood number (derived from the ratio of density difference to sum). This equation has been consistently found to fit the Rayleigh-Taylor instability in late time after it has become turbulent [2].

2.1.2 Richtmyer-Meshkov instability

We can extend our understanding of the Rayleigh-Taylor instability to that of the Richtmyer-Meshkov instability (RMI). From the vorticity argument for the instability it is obvious that all that is needed is $\nabla P \cdot \nabla \rho < 0$. The pressure term does not necessarily need to be constant as is for gravity, it can be impulsive as well. That is the case of the Richtmyer-Meshkov instability. In an instant, a large amount of vorticity gets deposited on the interface and the instability grows. The progression of the instability follows the progression of the constant acceleration case.

2.1.3 Transition to turbulence

The evolution of the Rayleigh-Taylor instability follows four main stages. Initially, if the perturbation amplitudes are small when compared to wavelength, the growth is exponential (following linear stability theory). Eventually, this will form spikes (fluid structures of heavy fluid growing into light fluid) and bubbles (fluid structures of light fluid growing into heavy fluid) from the individual sinusoidal modes on the interface. The growth of these structures can be modeled by using a

buoyancy drag model and the growth is linear in time (the velocity is constant); this is the second stage [3]. At this time, non-linear terms in the equations of motion can no longer be ignored and mode-coupling will begin to play a role. Then, the spikes and bubbles interact with each other through bubble merging and competition, where fluid structures merge to create larger structures and larger structures envelop smaller ones respectively; this is the third stage. This eventually develops into a region of turbulent mixing, which is the fourth and final stage.

The mixing region that develops is believed to be self-similar and turbulent if the Reynolds number is large enough [4]. **Figure 5** represents the evolution of the Rayleigh-Taylor instability from small wavelength perturbations at the interface.

The turbulent mixing that takes place represents active-scalar, level 2 mixing where the mixing is coupled to the flow dynamics [4]. The flow is postulated to follow the model $h = \alpha A g t^2$, where h is the mixing layer width, $A \equiv \frac{\rho_2 - \rho_1}{\rho_2 + \rho_1}$ (the density contrast) is the Atwood number, g is the acceleration and t is time [5]. Under the self-similar hypothesis, the flow at different times has the same geometry and there is no obvious temporally constant length scale for the mixing region to be scaled with; the mixing layer width is only coupled to the length scales within the mixing region. Thus, the mixing layer width and the internal wavelengths increase in time and must grow proportionally with each other. Eventually, the range of scales within the mixing region form a sufficient inertial range for fully developed turbulence to be assumed. A derivation, through dimensional analysis, of this self-similarity is presented by Roberts [1]. A fully developed turbulent flow implies self-similarity, but since a self-similar flow does not necessarily imply turbulence,

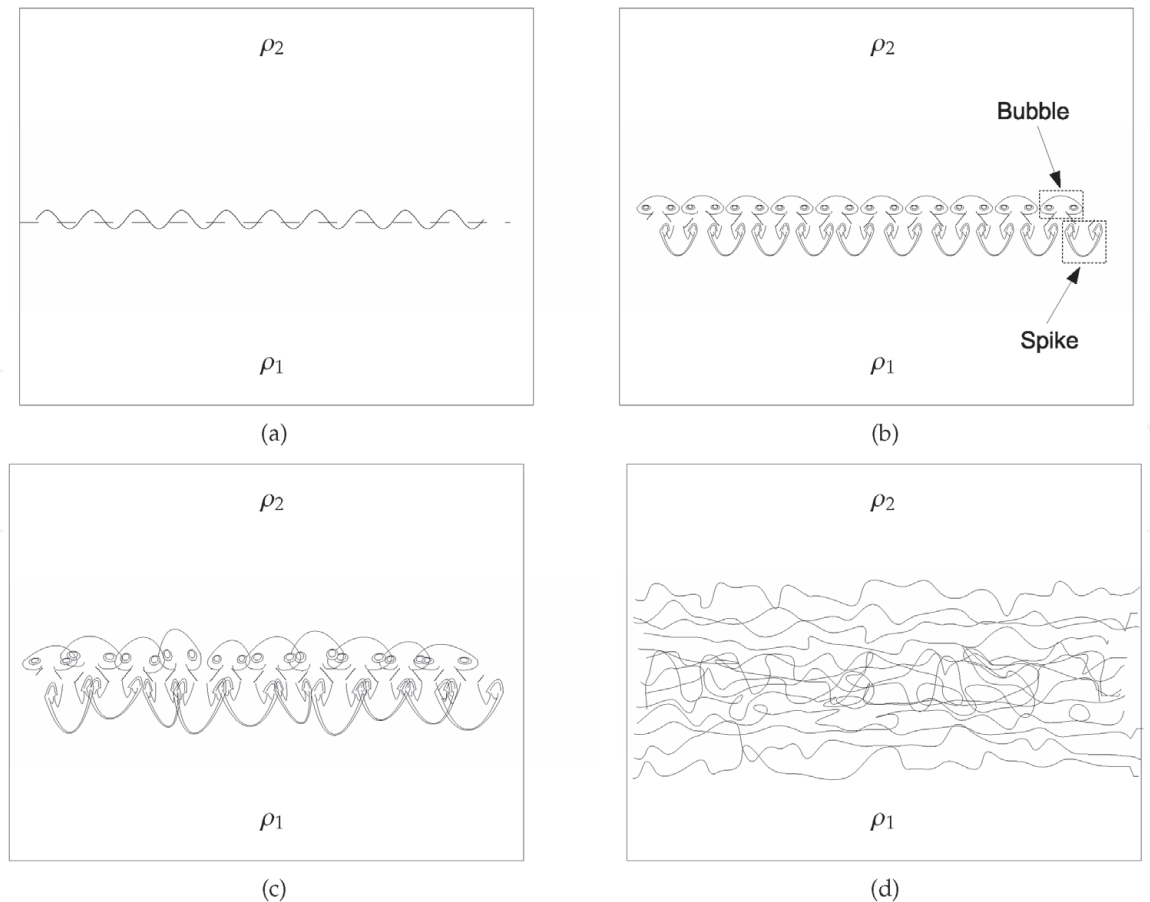


Figure 5. This figure represents the evolution of the Rayleigh-Taylor instability from small wavelength perturbations at the interface (a) which grow into the ubiquitous mushroom shaped spikes (fluid structures of heavy into light fluid) and bubbles (fluid structures of light into heavy fluid) (b) and these fluid structures interact due to bubble merging and competition (c) eventually developing into a mixing region (d) [1].

turbulence cannot be assumed without quantifying the statistical properties of the flow or by making comparisons to other studies where flow statistics are quantified.

When studying the mixing region produced by the Rayleigh-Taylor instability, discrepancies between experiments and simulations make it obvious that it is necessary to verify that fully developed turbulence is indeed being reached. One method of doing this is to look at the spectra and verify that it obeys the Kolmogorov $-5/3$ energy cascade in the inertial subrange. Also, with the loss of initial conditions that is indicative of turbulent flow, verifying the self-preserving behavior of the flow is a possibility.

2.1.3.1 Kolmogorov energy cascade

It is well accepted that fully developed turbulence displays the $k^{-5/3}$ dependence for the velocity spectrum. The same wavenumber dependence will be present in an initially smooth scalar field that is disturbed by the same turbulence [6], which is often more testable for the buoyancy-driven instabilities we have discussed. One method of testing this is by using a normalized power spectrum of the FFT of the concentration profiles and comparing to that of the Kolmogorov $-5/3$ law. It was observed by Dalziel et al. [7] that the RT instability roughly fits this and by Ramaprabhu and Andrews [8] as well.

2.1.3.2 Self-preservation

An important aspect of fully developed turbulence is the concept of self-preservation. In the case of the turbulent Rayleigh-Taylor instability this would require the various turbulent properties along the mixing zone to have a shape that maintains itself in time. When normalized by the proper scale, the curves should collapse on top of each other.

Comparison of self-similarity is a difficult task when it comes to experiment, but Ramaprabhu and Andrews [8] does this with the use of PIV measurements. It is indeed observed that when normalizing with mean velocity, there is a collapse of the curves for profiles in later time. This can also be observed by looking at the similarity of different concentration profiles in time (**Figure 6**) from the experiments of Roberts and Jacobs [2]. From the profile images the self-similarity becomes obvious, thus implying turbulence.

2.1.4 Linear stability theory

Linear stability theory is often used to derive equations governing the stability of a fluid system. It has been done many times in the past for the Rayleigh-Taylor instability. One such derivation is that done by Roberts which combines both the Rayleigh-Taylor and Richtmyer-Meshkov instabilities [9]. The way in which the derivation begins, is by considering a slightly perturbed interface and plugging this into the Navier-Stokes equations. By assuming small perturbations of the interface, simplifications can be made since squares of small values should be neglected. The full derivation will not be performed here, just some notable points for discussion.

We consider two stratified incompressible fluids where the interface is assumed infinitesimally thin and a sinusoidal disturbance is imposed upon it, in both the x and y directions, as displayed in **Figure 7**. Since each fluid region is considered to be initially at rest, they are irrotational. Here vorticity can only be introduced at the boundaries (in this case the interface) and then transmitted into the rest of the flow by viscous diffusion.

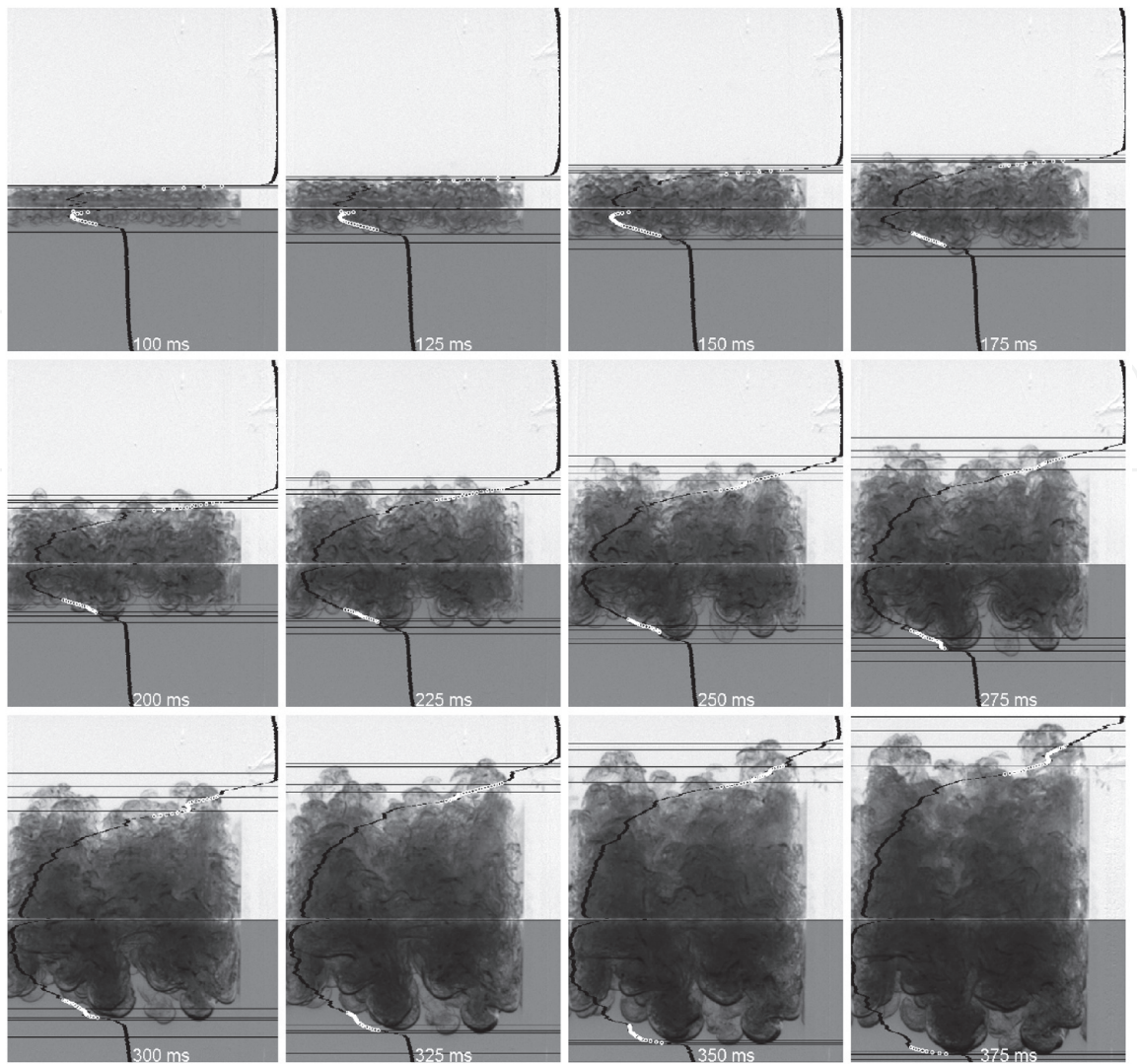


Figure 6.
 From the experiments of Roberts and Jacobs [2], an experimental sequence of images where the images of an ensemble average of many experiments is shown progressing in time. Horizontally averaged intensity values are superimposed on the images. The profiles have the characteristics of a self similar flow as time progresses.

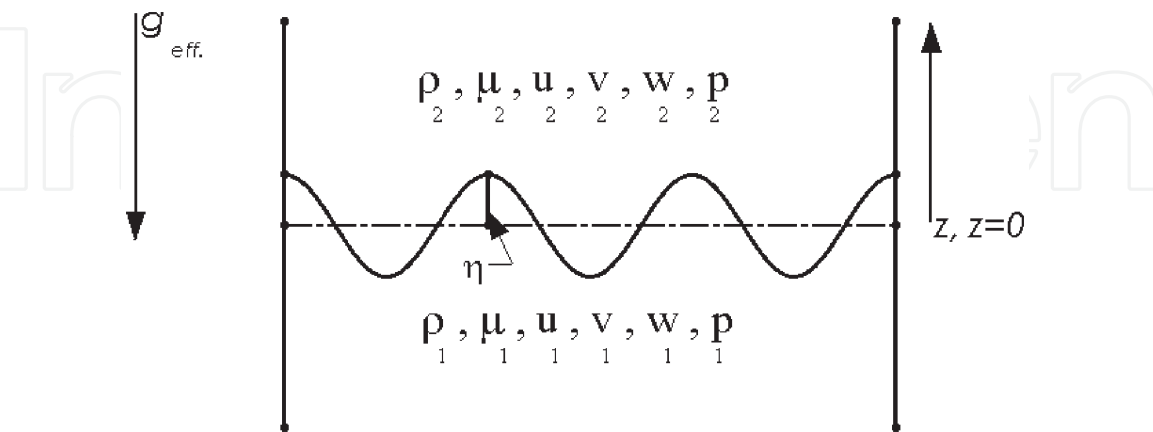


Figure 7.
 Interface representing our fluid configuration [1].

Considering diffusion effects to be confined to the infinitesimally thin interface we can say that the fluid is irrotational throughout the two regions. By using the potential functions: $u = \frac{\partial \phi}{\partial x}$, $v = \frac{\partial \phi}{\partial y}$ and $w = \frac{\partial \phi}{\partial z}$ (where ϕ is a function of x, y, z and t), one can then derive the continuity equations for the two fluid regions. In general on

the interface there is surface tension and this can give us an equation relating the pressure at the interface. This taken with the geometry of the interface itself gives an interfacial boundary condition. Since we are considering the flow to be irrotational, we can use the unsteady Bernoulli equation for each fluid region to solve the equations. After much equation manipulation one can arrive at the well known linearized stability ODE,

$$\ddot{a} - \left[\frac{\rho_2 - \rho_1}{\rho_2 + \rho_1} - \frac{\gamma k^2}{(\rho_2 + \rho_1)g_{\text{eff}}} \right] kg_{\text{eff}} a = 0, \quad (9)$$

where a is the acceleration of the interface due to the fluid flow, $\rho_{2,1}$ represents the density of the upper and lower fluids respectively, γ is the surface tension, g_{eff} is the effective gravity and k is the wavenumber (2π over the wavelength). By neglecting surface tension, one can simplify the expression to,

$$\ddot{a} - Ak g_{\text{eff}} a = 0. \quad (10)$$

This equation applies both to the Rayleigh-Taylor and Richtmyer-Meshkov instabilities.

2.1.4.1 Rayleigh-Taylor instability

In Eq. (10), when considering a constant acceleration for g_{eff} , we have an ODE that represents the R-T instability. This is a second-order ODE and can be solved easily.

Representing $\sigma^2 = kAg_{\text{eff}}$ we arrive at

$$a = C_1 e^{\sigma t} + C_2 e^{-\sigma t}. \quad (11)$$

If $Ag_{\text{eff}} < 0$, σ is imaginary and therefore the equation yields a stable condition. If $Ag_{\text{eff}} > 0$, σ is real and therefore the equation is unstable (it grows in time).

This equation can also be represented in a better way in which the coefficients represent the initial amplitude and velocity of the sinusoidal disturbance,

$$a = a_0 \cosh(\sigma t) + \dot{a}_0 \sinh(\sigma t). \quad (12)$$

2.1.4.2 Richtmyer-Meshkov instability

Eq. (10) can also be considered when g_{eff} is an impulsive acceleration defined by $g_{\text{eff}} = \delta(t)V$, where V is the velocity produced by the impulse.

This can be integrated to yield

$$\int_{a_0^-}^{a_0^+} \ddot{a} = AkV \int_{t^-}^{t^+} a \delta(t) d\tau, \quad (13)$$

where

$$a_0 = a(0). \quad (14)$$

$$\Rightarrow \dot{a} = AkVa_0 + \dot{a}(0).$$

by integrating once more we acquire

$$a = AkVa_0t + \dot{a}_0t + a_0 \Rightarrow a = a_0(kAVt + 1) + \dot{a}_0t. \quad (15)$$

2.1.5 Small wavelength damping and stabilization

The effects of viscosity act only at small scales in RT instability and therefore act to select particular wavelengths as opposed to others. Since viscosity only acts at small scales, its effect can be neglected once the instability has become larger than these scales. This can be understood by comparing the terms of RT growth with that of viscous damping. First, The RT growth term from inviscid theory is $e^{\sqrt{kAg_{\text{eff}}}t}$ [9] and that of viscous damping is $e^{-2\nu k^2t}$ [10]. It is of interest here to see when the RT growth term is much larger than the viscous term,

$$e^{\sqrt{kAg_{\text{eff}}}t} > e^{-2k^2\nu t}. \quad (16)$$

This yields

$$k < \sqrt[1/3]{\frac{Ag_{\text{eff}}}{4\nu^2}}. \quad (17)$$

Eq. (17) gives us a way to calculate an approximate wavelength at which larger than which we can ignore viscosity effects. As an example, with water and air at room temperature, $k = 13,485$. This translates to a wavelength of approximately 0.46 mm. The dominant scales that we are measuring are certainly larger than this, so for this regime we can neglect viscous effects. Next, for completeness the RT growth from the self-similar model will be compared to the viscous damping term. Again, let us examine when the RT growth is a lot larger than the viscous damping,

$$\alpha Ag_{\text{eff}}t^2 > e^{-2k^2\nu t}. \quad (18)$$

This yields

$$k < \sqrt{\frac{\ln(\alpha Ag_{\text{eff}}t^2)}{-2\nu t}}. \quad (19)$$

As an example, from the experiments of Roberts and Jacobs [2], by assuming an approximate α value of 0.05 and a time of 300 ms (this time corresponds to the beginning of the measurable mixing region development in their experiments) we conclude that the wavenumbers should be less than approximately 2500 (2.5 mm). This does fall in line with the small wavelengths and structures we observe in the images shown previously.

Keep in mind, this is an approximation to the viscous effects where a viscous damping was used. If a detailed analysis is necessary to determine the fastest growing wavelength, the derivations of Chandrasekhar [11] will give a more detailed explanation and more exact solution.

Another damping effect at small wavelengths is that due to interfacial tension. We use the term interfacial tension here to be more general, but the most obvious example of this is surface tension where there is a free surface - such as in the air water interface created in a glass of water or a straw. Interfaces of oil and water will also have an interfacial tension which will act to shift the fastest growing wavelength to the larger

scales by damping out smaller scales as well as viscosity. However, interfacial tension has more than just a damping effect but actually has a stabilizing effect, such that there becomes a critical wavelength smaller than which the instability will not grow.

2.1.6 Applications

The classic observation of the Rayleigh-Taylor instability is the simple inversion of a glass of water. Due to gravity, air (the less dense fluid) moves into the water (the more dense fluid) and the instability develops as a consequence of perturbations at the interface (as typically is in a natural environment). If one were to look at simple fluid statics, the water should not “fall” out. Since the bottom of the glass is covered, atmospheric pressure should hold the water in place when fluid statics alone is considered; this does not take place because of the instability. An interesting phenomenon is that of a covered straw with water in it. The same configuration is present, however the water stays in place. By considering surface tension, we must recognize that it has a stabilizing affect on the instability for smaller wavelengths. The diameter of the straw is often smaller than the critical wavelength and therefore nothing larger can develop and the wavelengths that do are not unstable. This has implications for any engineering applications that rely on gravity. If the diameter is too small, you cannot rely on the presence of the instability to assist and you would need to account for the pressure difference given by fluid statics and atmospheric pressure. An extension of this example can be made to the Richtmyer-Meshkov instability. With the straw example, instead of just allowing the water to remain under gravity, you can shake the straw thus creating impulsive accelerations that (if strong enough) may shift the critical wavelength low enough such that the flow becomes unstable and the liquid flows out. The same can be thought of for the bottle of ketchup that needs that impulsive acceleration to start flowing. Although the physics of the ketchup are more complicated since it is a non-Newtonian fluid, at least at the beginning of the flow, RM instability plays a role. The extension here to our pipe under gravity example would be that in a situation where some external pressure differential is applied, but not necessarily enough to overcome atmospheric pressure and the diameter of the pipe is too small for the RT instability alone to work, pulsing the pressure source might help trigger a RM instability.

A more natural occurrence of these instabilities is in supernovae. Here, there are stratified gases of different density. This difference in density arises from the fact that the gas closer to the center is hotter (and therefore less dense), due to its proximity to the burning fuel, than the gas farther from the center. This, in addition to the outward acceleration that was produced by the explosion (both impulsive and constant), creates unstable RT and RM configurations [12]. This in turn will generate mixing which will alter the way in which the flow progresses and how heat is distributed. Astronomers can use this information to better understand and find these phenomena. In relation to studying the stars, RTI also shows up when we explore them. Hall-effect thrusters are becoming very popular for space flight (especially satellites) due to their large specific impulse. In these thrusters, the wall at the thruster exit has been shown to erode due to the instability and therefore a better understanding is necessary [13]. We also see RTI in salt domes. Here, the less dense salt that is buried beneath more dense sediment experiences an upward acceleration due to gravity [14]. Although the timescales and effective viscosities are very large, this still forms a RTI on geologic timescales.

Another important application is inertial confinement fusion (ICF), which if mastered would lead to cheap and plentiful energy from water. In ICF, a capsule containing a Deuterium/Tritium (DT) mixture is bombarded with energy originating from high powered lasers with the purpose of causing a fusion reaction to take place;

the two isotopes fuse producing He_4 , a neutron and energy [15]. ICF experiments are currently being performed at the National Ignition Facility (NIF) in Lawrence Livermore National Laboratory (LLNL). The ICF capsule is a sphere comprised of three main layers. The outer shell is an ablator material made from plastic doped with other elements such as Beryllium or Germanium. Interior to that is a layer of DT ice surrounding DT gas. There are two main types of ICF, direct and indirect drive. In direct drive, lasers directly irradiate the target. In indirect drive, lasers enter a hohlraum which has the capsule in the center. The hohlraum is a hollow cylinder that is composed of a high Z (large atomic number) material, such as gold. The lasers irradiate the inside of the hohlraum which re-emits the energy as x-rays. In the indirect drive method, a more uniform energy distribution is deposited on the ablator layer. The energy deposited on the ablator causes it to blow off, and by Newton's third law, PdV work is done on the interior of the capsule. The compression of the DT gas region results in an increase in pressure at the center of the capsule causing very high temperatures to develop. In addition, shocks (caused by the ablation) pass into the DT gas region, which also add to the pressure and temperature rise. The pressure rise at the center eventually acts to decelerate the initially accelerating implosion until a stagnation point is reached [16]. This "hot spot" will reach the conditions for thermonuclear burn if a high enough temperature is achieved. During this process, there are two ways in which the Rayleigh-Taylor and Richtmyer-Meshkov instabilities can develop which acts to mitigate ignition and decrease total yield.

Firstly, RTI and RMI can occur at the interface of the outer ablator shell (after becoming a plasma) and the DT ice layer during the initial implosion of the target. In this configuration, the smaller density of the outer ablator plasma layer and the larger density DT ice inner layer create an inward acting density gradient. This in conjunction with the outward acting pressure gradient results in an RT/RM unstable configuration. By choosing layers of gradually varying density with different dopants such as Germanium, for the ablator material, the density difference can be decreased; thus, decreasing RT growth. Also, by using indirect drive (to produce a more uniform energy deposition), the effect of the instabilities can be minimized as well by effectively decreasing the perturbations necessary to begin the instability. The second way that RTI and RMI can occur is during the deceleration phase between the high temperature, high pressure DT gas and the outer, colder DT ice layer. Here, the pressure gradient is directed inward and the density gradient is directed outward which is also an RT/RM unstable configuration. The RTI generated in both these instances causes mixing. This mixing brings cold fuel from the outer layer into the center "hot spot," lowering the temperature and decreasing the reaction rate; this process may prevent ignition altogether [17]. By more fully understanding this instability, more efficient capsules can be designed. In addition to this, other methods to control the onset of RTI in fusion experiments using rotating magnetic fields is being studied [18].

There are some situations where one does not want to prevent these instabilities from forming at all, but actually want to encourage it and the increased mixing that happens from it. One such example for RMI is that for a scramjet. With scramjets (supersonic combustion ramjets), we wish to do combustion at supersonic speeds. This is as opposed to standard ramjets in which the flow is slowed in the engine so that proper mixing can occur. To accomplish this in scramjets, RMI is utilized to enhance the mixing [19]. The geometry of the engine can be configured to create shockwaves that will interact at specific fuel/air boundaries; this will impart impulsive accelerations that trigger RMI and eventually turbulent mixing. This extra mixing is necessary to get a proper fuel/air mixture.

As can be observed, there are many applications to studying these instabilities to control, prevent or encourage their growth.

2.2 Shear-driven instabilities

Another class of stratified instabilities is shear-driven ones—where there is a difference in shear forces across the interface for instance. One such instability is the Kelvin-Helmholtz instability that happens if there is a jump in velocity across an interface. From Eq. 4, we see that if the velocity gradient is large enough, then a stabilizing buoyancy instability effect will be overcome and we will have vorticity deposited. $\frac{1}{\rho^2} \nabla \rho^2 \times \nabla P + \frac{\partial U_x}{\partial y} \frac{u_x}{\partial x} > 0$. As can be seen in **Figure 8**, when we ignore the effects of buoyancy, a velocity difference between top and bottom fluid (a gradient in the direction orthogonal to the flow) will create vorticity due to the torque from a perturbed interface. If a U_2 is larger than U_1 , this vorticity will create even more shear, which will create more vorticity. This instability can be observed in clouds when there is stratification with high velocity present or even when one pours a bottle of oil and vinegar salad dressing. Another interesting application of this instability is in semiconductor manufacturing where the ion beams used in chemical vapor deposition and ion implantation becomes subjected to this instability [20].

3. Baroclinic instability

All of the instabilities mentioned so far often occur in nature as there are often stratified flows in the atmospheres and oceans. Another extension of this is on the much larger geophysical scale, where the Coriolis force due to the earth rotation and velocity difference at different lines of latitude as the radius with the rotation axis varies. In this configuration, we have both the hydrostatic balance $\frac{\partial p}{\partial z} = \rho g$ and the geostrophic balance $2\Omega \sin \theta U = -\frac{1}{\rho} \frac{\partial p}{\partial y}$, where Ω is the earth's rotation and density ρ is a function of temperature (**Figure 9**).

It is then determined that for instability that, $\frac{H \sqrt{-\frac{g}{\rho_0} \left(\frac{\partial p}{\partial y} \right)}}{\Omega}$ [21], where H is the height in the vertical and $\frac{\partial p}{\partial y}$ is the pressure gradient due to a temperature gradient. As can be observed, there are very specific conditions for this instability to develop. If the temperature gradient is too small or too high, this particular instability will not develop, but also a part of this is the vertical height and the earth's rotation. This instability shows up quite often as the development of vorticity in the earth's oceans and atmosphere and is a large contributing factor to weather patterns.

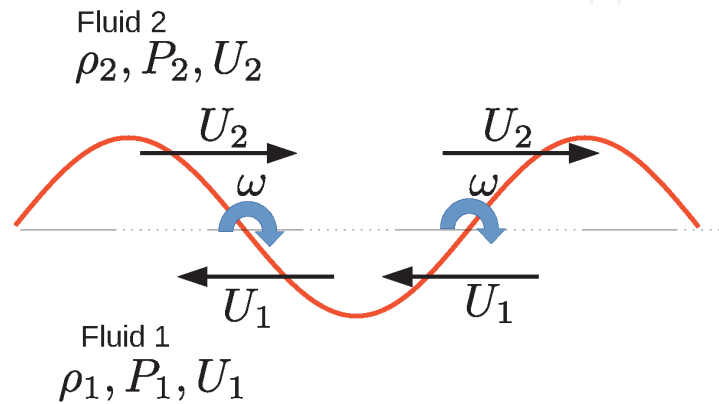


Figure 8.

Vorticity created when there is velocity gradient in the base flow and a perturbed interface. It is clear here that a torque would be created when the interface is misaligned.

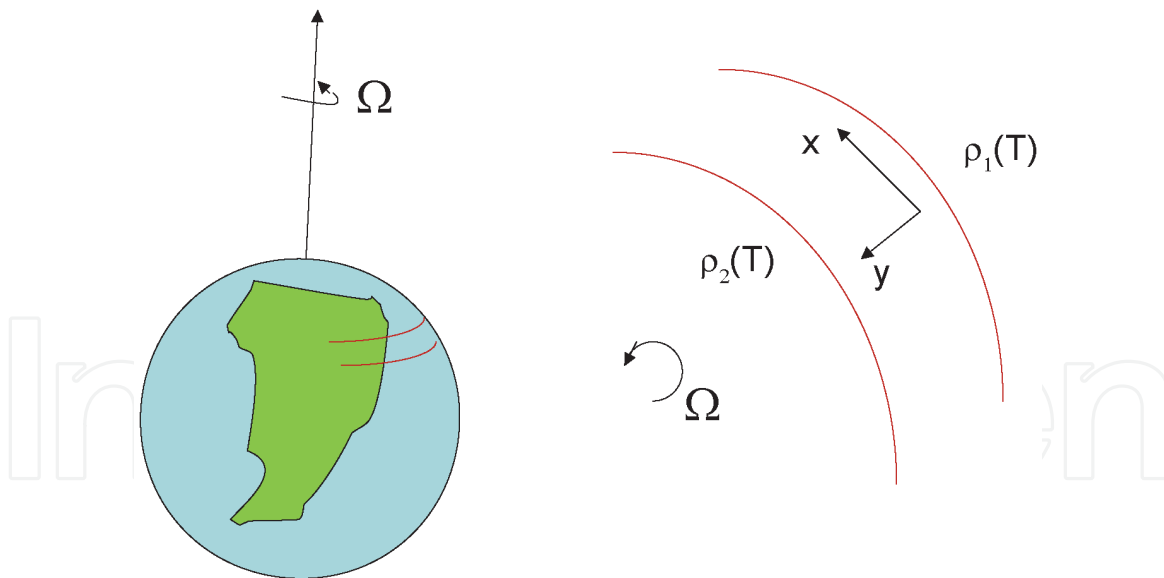


Figure 9.
 The rotation of the earth sets up a situation in which instability can occur due to the combined action of the hydrostatic and geostrophic balances.

4. Parallel shear flow instability

A very broad and far reaching class of flows is that of parallel shear flows. These are flows that are mostly unidirectional and have velocity profiles created by the no slip condition at the boundary. This includes and has historically been studied for pipe flow by Reynolds [22]. The flow can also be extended to that of unbounded flows and even base flows in which there is a slight curvature, but parallel to a first-order approximation, such as flow over a wing. Under certain conditions, these flows can become unstable leading to turbulence and separation which has implications to engineering design. First, we will consider inviscid flow and then discuss viscosity effects.

4.1 Inflection points and adverse pressure gradients in inviscid flow

It was Rayleigh [23] who first recognized the importance of inflection points in the velocity profile. He proposed that for instability to be present, a necessary condition is an inflection point in the velocity profile. This was expanded upon by Fjørtoft [24] who proposed that another necessary condition for instability is that $\frac{\partial^2 U}{\partial z^2} (U - U_s) < 0$ somewhere in the flow where z_s is a point at which $\frac{\partial^2 U}{\partial z^2} = 0$ and $U_s = U(z_s)$ [25]. This basically means that in a velocity profile, not only does there need to be an inflection point (change in curvature or where it goes from concave up to down or vice versa), also, if you follow along the profile, at some points in the flow, the difference in velocity there to that at the inflection point times the curvature should be negative. This typically happens when there is an adverse pressure gradient (pressure that pushes in the opposite direction of the flow). In this situation, the velocity profile starts as one would expect (bulging forward), but it eventually starts bulging backwards which is unstable and can lead to flow separation in an unbounded flow.

One way that an inflection point occurs is with an adverse pressure gradient. In pipe/duct flow this can be difficult to realize if the main flow is caused by a pressure gradient. However, we can have a situation where a localized pressure gradient (caused by a fan or impeller) creates a forward moving velocity profile, but there is

back pressure in the over all configuration that will make an unstable flow configuration. Adverse pressure gradients are a bit more obvious with unbounded flows. We can start by looking at the boundary layer equation,

$$u \frac{\partial u}{\partial x} + v \frac{\partial u}{\partial y} = -\frac{1}{\rho} \frac{\partial p}{\partial x} + \nu \frac{\partial^2 u}{\partial y^2} \quad (20)$$

where the pressure gradient is based has the form from the base flow as $-\rho U \left(\frac{dU}{dx} \right)$. In this situation, at the wall (due to the no slip condition and continuity equation), we have zero velocity components which yields,

$$\mu \left(\frac{\partial^2 u}{\partial y^2} \right)_{wall} = \frac{\partial p}{\partial x}. \quad (21)$$

Therefore, in the immediate vicinity of the wall, the curvature of the velocity profile is dictated by whether the pressure gradient is positive or negative. Thus, an adverse pressure gradient will lead to an inflection point. Over a wing, what creates lift (and a pressure gradient in the y direction) is streamline curvature. The streamlines must curve to fit the body at first, but this also means that toward the trailing edge they must then curve back to the background stream, and there will be an adverse pressure gradient. Decreasing the degree of curvature over the trailing edge will decrease the magnitude of the adverse pressure gradient and thus prevent separation further along the wing, thus minimizing drag. In addition, “tripping” the boundary layer by making it turbulent early on also prevents separation as there is more momentum in the flow giving a wider velocity profile that can withstand an adverse pressure gradient longer.

4.2 Orr-Sommerfeld equation

The criteria for stability so far have been considered for inviscid flow. To extend this to include viscosity as well does make the equations much more complicated. We will not derive this here. It can be derived by using linear stability theory on the Navier-Stokes equations as done by Cohen and Kundu [21] yielding the result,

$$(U - c) \left(\frac{\partial^2 \phi}{\partial y^2} - k^2 \phi \right) - \frac{\partial^2 U}{\partial y^2} \phi = \frac{1}{ikRe} \left[\frac{\partial^4 \phi}{\partial y^4} - 2k^2 \frac{\partial^2 \phi}{\partial y^2} + k^4 \phi \right], \quad (22)$$

where c is the wave speed, k is the wavenumber and ϕ is defined such that the perturbation velocities, $u = \frac{\partial \phi}{\partial y}$ and $v = -ik\phi$. As can be observed, this is a fourth-order differential equation which is very difficult to solve. The only way to approach such a problem would be to solve this equation a numerical simulation. Since it is an ordinary differential equation, there are many methods that can be used. But, better yet is to use one of the inviscid simplifications discussed previously.

4.3 Engineering applications

Parallel shear flows have become some of the most obvious flows around us and thus have strong engineering importance. From pipe flow to flow over wings and cars there is great importance. With flow in pipes, it was noticed by Rayleigh [23] that turbulent spots develop above a certain Reynolds number and then eventually the flow becomes fully turbulent. This happens at a Reynolds number of approximately 3000. This is important to take note of as a turbulent flow will be noisier and

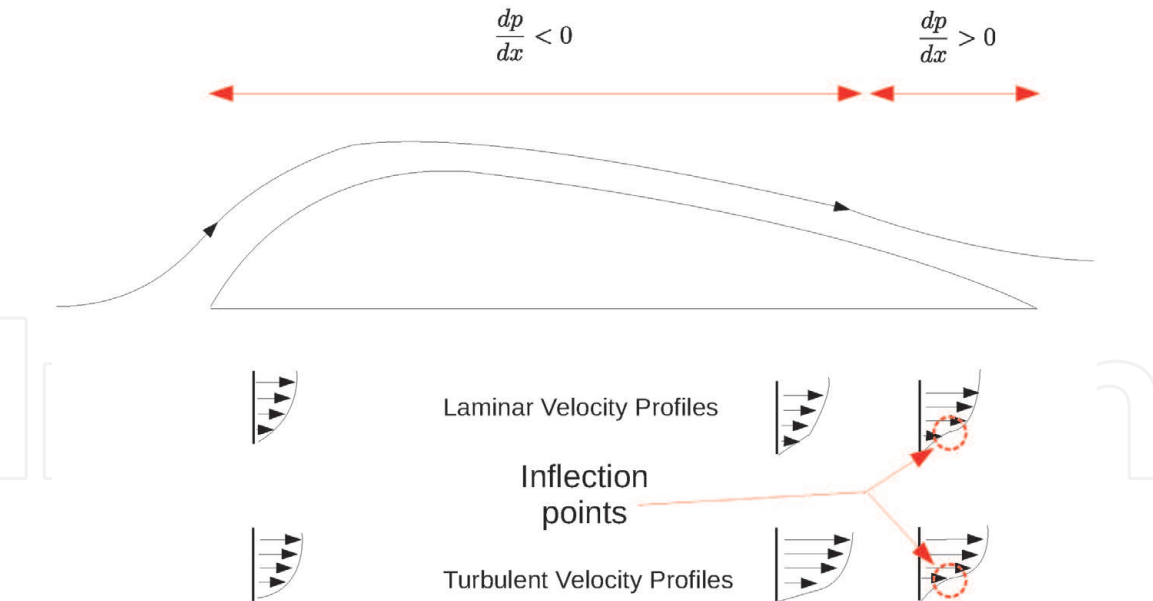


Figure 10.
Initially, the flow is in a favorable pressure gradient, but this eventually changes to adverse one where an inflection point forms in the velocity profile and the flow is in danger of separation which would increase drag. The top row of velocity profiles represent that for laminar flow, whereas the bottom row represents that for a turbulent flow which is seen to be fuller and thus less susceptible to backflow.

the extra flow non-uniformity can lessen the life of pipes. For flow over bodies, we have to also look at the pressure gradient and whether it is adverse or not. An adverse pressure gradient will eventually lead to separation, but this can be delayed if the flow is turbulent. This means, that although we need to locally introduce irregularities in the flow to induce turbulence, at the same time we would want to minimize the adverse pressure gradient to prevent separation (which will in turn increase drag). A pictorial representation of a simplified view of the flow over the wing is shown in **Figure 10**.

As can be observed from the flow over a wing, at first there is a favorable pressure gradient, which eventually turns into an adverse pressure gradient at the trailing edge. In order to make lift, we want to have a pretty large wing curvature at first (this creates the pressure gradient perpendicular to the wing that creates lift), but then we can smoothly allow the wing and streamlines transition to free stream to try and push back the section where we have an adverse pressure gradient. In this adverse pressure gradient region is where the velocity profile can get an inflection point which could eventually lead to back flow in the velocity profile and flow separation. Once the flow separates, you will have increased pressure drag as there will be a low pressure region in this separated trailing edge region. It also turns out that since turbulent boundary layers are fuller and have more momentum, it takes longer for an inflection point to create backflow and therefore the flow stays attached longer. One can “trip” the boundary layer (by depositing a small amount of vorticity in the flow right in the boundary layer (small triangular surfaces seen on a wing’s leading edge) such that the boundary layer becomes turbulent, but the rest of the flow does not.

5. Conclusions

Fluid instabilities show up everywhere in nature. In this chapter we have discussed some of the main instability classes. Stratified fluid flows were discussed first as it is in some ways the simplest to understand. They show up in our coffee,


our condiments, in the atmosphere and the oceans, basically wherever there is a density difference present between the two layers. Depending on the orientation of the density difference, vorticity can be generated in a self-sustaining process. Using linear stability theory, it is determined how different wavelengths grow at different rates for the system and how interfacial or surface tension acts has a stabilizing effect. One can also look at the effects of viscosity which has a damping effect on the smaller wavelengths, thus giving rise to a fastest growing wavelength which has direct implications to engineering applications as the geometry of the system can act to directly prevent or create these wavelengths, therefore controlling instability growth. Once the instability has grown enough, the linearized equations no longer hold and non-linear effects including interactions between structures will take place. This eventually leads to turbulence. This instability can then be extended to include the case where instead of a density difference at an interface, there is a velocity difference causing what is known as shear-driven instabilities. Once these two base instabilities are discussed, it is an easy extension to that of the baroclinic instability which is a primary cause of many of the earth's weather patterns. Due to interactions of velocity and density gradients (caused by temperature gradients), it is a natural extension to the previously discussed instabilities. From this, the more complicated case of parallel shear flows was discussed. This includes flow over wings and flows in pipes. In this case, first the stability criteria was discussed, but then extended to the full Orr-Sommerfeld equation, where unlike linear stability theory, does not remove viscosity from its initial derivations and allows for non-linear effects. Here we discuss instability more as an eventual path to turbulence and how controlling, preventing and even creating it can be advantageous to reducing drag, or preventing noise. In this chapter, much was covered but a broad understanding of how different fluid instabilities all relate together and can be understood to thus control them when designing and running our engineering systems.

Author details

Michael S. Roberts
University of Arizona, Tucson, AZ, USA

*Address all correspondence to: [window59@hotmail.com](mailto>window59@hotmail.com)

IntechOpen

© 2020 The Author(s). Licensee IntechOpen. This chapter is distributed under the terms of the Creative Commons Attribution License (<http://creativecommons.org/licenses/by/3.0>), which permits unrestricted use, distribution, and reproduction in any medium, provided the original work is properly cited. 

References

- [1] Roberts MS. Experiments and simulations on the incompressible, Rayleigh-Taylor instability with small wavelength initial perturbation [Dissertation]. The University of Arizona; 2012
- [2] Roberts MS, Jacobs JW. The effects of forced small-wavelength, finite-bandwidth initial perturbations and miscibility on the turbulent Rayleigh-Taylor instability. *Journal of Fluid Mechanics*. 2016;**787**:50-83
- [3] Oron D, Arazi L, Kartoon D, Rikanati A, Alon U, Shvarts D. Dimensionality dependence of the Rayleigh-Taylor and Richtmyer-Meshkov instability late-time scaling laws. *Physics of Plasmas*. 2001;**8**(6):2883-2889
- [4] Dimotakis PE. Turbulent mixing. *Annual Review of Fluid Mechanics*. 2005;**37**:329-356
- [5] Youngs D. Numerical simulation of turbulent mixing by Rayleigh-Taylor instability. *Physica D*. 1984;**12**:32-44
- [6] Tennekes H, Lumley JL. *A First Course in Turbulence*. Massachusetts, USA: MIT Press; 1972
- [7] Dalziel SB, Linden PF, Youngs DL. Self-similarity and internal structure of turbulence induced by Rayleigh-Taylor instability. *Journal of Fluid Mechanics*. 1999;**399**:1-48
- [8] Ramaprabhu P, Andrews MJ. Simultaneous measurements of velocity and density in buoyancy-driven mixing. *Experiments in Fluids*. 2003;**34**(1):98-106
- [9] Roberts MS. Experiments on the miscible liquid Rayleigh Taylor and Richtmyer Meshkov instabilities [master's thesis]. University of Arizona; 2006
- [10] Lamb H. *Hydrodynamics*. New York, USA: Dover Publications; 1932
- [11] Chandrasekhar S. *Hydrodynamic and Hydromagnetic Stability*. New York, USA: Dover; 1961
- [12] Kifondis K, Plewa T, Scheck L, Janka HT, Muller E. Non-spherical core collapse supernovae. *Astronomy and Astrophysics*. 2006;**453**(2):661-U17
- [13] Malik HK, Tyagi J, Sharma D. Growth of Rayleigh instability in a Hall thruster channel having dust in exit region. *AIP Advances*. 2019;**9**:055220
- [14] Selig F, Wermund EG. Families of salt domes in the gulf coastal province. *Geophysics*. 1966;**31**(4):726-740
- [15] Ghasemizad A, Zarringhalam H, Gholamzadeh L. The investigation of Rayleigh-Taylor instability growth rate in inertial confinement fusion. *Journal of Plasma Fusion Research*. 2009;**8**:1234-1238
- [16] Betti R, Umansky M, Lobatchev V, Goncharov VN, McCrory RL. Hotspot dynamics and deceleration-phase Rayleigh-Taylor instability of imploding inertial confinement fusion capsules. *Physics of Plasmas*. 2001;**8**(12):5257-5267
- [17] Mccrory RL, Verdon CP, Betti R, Goncharov VN. Growth rates of the ablative Rayleigh-Taylor instability in inertial confinement fusion. *Physics of Plasma*. 1998;**5**(5):1446-1454
- [18] Zhu G, Shi P, Yang Z, Zheng J, Luo M, Ying J, et al. A new method to suppress the Rayleigh-Taylor instability in a linear device. *Physics of Plasmas*; **26**: 2019, 042107
- [19] Neill SM, Pesyridis A. Modeling of supersonic combustion systems for sustained hypersonic flight. *Energies*. 2017;**10**:900
- [20] Rani K, Sharma SC. Theoretical modelling of Kelvin Helmholtz

instability driven by an ion beam in a negative ion plasma. Progress in Electromagnetics Research B. 2016;**71**: 167-181

[21] Cohen IM, Kundu PK. Fluid Mechanics. 3rd ed. California, USA: Elsevier Academic Press; 2004

[22] Reynolds O. An experimental investigation of the circumstances which determine whether the motion of water shall be direct or sinuous and of the law of resistance in parallel channels. Proceedings of the Royal Society of London. 1883;**35**:84-99

[23] Lord Rayleigh FRS. On the stability, or instability, of certain fluid motions. Proceedings of the London Mathematical Society. 1879;**s1-11**(1): 57-72

[24] Fjørtoft R. Application of integral theorems in deriving criteria of stability for laminar flows and for the baroclinic vortex. Geofys Publ. Oslo. 1950;**17**(6): 1-52

[25] Drazin PG, Reid WH. Hydrodynamic Stability. Cambridge, UK: Cambridge University Press; 1981